Bonn-Gatchina partial wave analysis

A. Sarantsev[1)]

(Petersburg Nuclear Physics Institute, Gatchina, 188300, Russia)
(Helmholtz Institut für Strahlen und Kernphysik, Bonn, 53115, Russia)

Abstract The present status of the Bonn-Gatchina partial wave analysis of the photoproduction and pion induced data is presented. An observation of signals which can be associated with new baryon resonances and possible interpretations of the baryon spectrum is discussed.

Key words baryon, photoproduction, K-matrix analysis

PACS 11.80.Et, 11.80.Gw, 13.30.-a

1 Introduction

The flavor structure of baryon resonances is well described in quark models which assume that baryons can be build from three constituent quarks. The spatial and spin-orbital wave functions can be derived using a confinement potential and some residual interactions between constituent quarks. The best known example is the Karl-Isgur model[1], at that time a breakthrough in the understanding of baryons. Later refinements differed by the choice of the residual interactions: Capstick and Isgur continued to use an effective one gluon exchange interaction[2], Plessas and his collaborators used exchanges of Goldstone bosons between the quarks[3], while Löring, Metsch and Petry exploited instanton induced interactions[4]. A group theoretical analysis by Bijker, Iachello and Leviatan gave the same complexity of the spectrum of baryon resonances[5]. Quark models, including a discussion of different decay modes, were reviewed recently by Capstick and Roberts[6].

A common feature of these models is the large number of predicted states: the dynamics of three quarks leads to a rich spectrum, much richer than observed experimentally. The reason could be that the dynamics of three quark interactions is not understood well enough. It is often assumed for instance that, within the nucleon, two quarks may form a diquark of defined spin and isospin, and that the diquark is a 'stable' object within the baryon. Applied to baryon spectroscopy, the diquark model helps to solve the problem of the missing baryon resonances.

Of course, there is also the possibility that symmetric quark models treating all three quarks on the same footing are right, and that the large number of predicted but unobserved states reflects an experimental problem.

Most properties of baryon resonances have been derived from $\pi^{\pm}$p elastic scattering and from the $\pi^{-}\mathrm{p} \to \mathrm{n}\pi^{+}$ charge exchange reaction[7] . Over a wide energy range, differential cross sections covering nearly the full angular range were determined as well as the asymmetry in the distribution of the scattering plane when the target proton was polarized.

The most recent results of the SAID group[8] are based on a large data sample and masses and widthes of the leading four-star resonances mostly agree with the older results. For the other resonances, the results differ dramatically; if true they require to reconsider our understanding of the baryon spectrum. For example the new analysis did not find any indications for the $P_{33}(1600)$ and $P_{11}(1710)$ states which are predicted by all existent models.

Quark model calculations predict that high-mass resonances have small branchings to the Nπ channel which enter with the second power into the elastic cross section. Inelastic reactions like photoproduction of multi-meson final states offer therefore an independent approach to baryon spectroscopy.

The amplitudes for photoproduction of mesons contains of course more information than just pole position and residues. In this paper we present ampli-

Received 7 August 2009

1) E-mail: andsar@hiskp.uni-bonn.de

tudes for photoproduction of pions which are compared to those given by SAID and MAID.

For the most important waves, the πN elastic scattering partial wave amplitudes from[8] are included in the analysis. The missing information about inelastic channels is derived from photoproduction data: the inelasticity in πN scattering due to couplings of a given baryon resonance to other final states like e.g. ΣK is related to the contribution of this resonances to $\gamma p \to \Sigma K$ and $\gamma p \to N\pi$.

The analysis presented here aims at a coupled channel analysis of all reactions relevant for baryon spectroscopy. There are, however, some practical limitations to the desired "all data". Different data sets can contradict each other. In the data selection, we follow the GWU Data Analysis Center but exclude some older data when new precision data have become available. There are discrepancies between Saphir and CLAS data on strangeness production; it was shown that both data sets can be fitted simultaneously when an energy-dependent normalization factor is admitted. Here, we use the CLAS data with its higher statistics. There are some discrepancies in π^0 photoproduction between CBELSA and CLAS in forward angles; we use the data alternatively. The only significant change we find is in the t-channel exchange contribution. In the present stage of the analysis, we do not include vector mesons nor data on pion- or photon-produced Nππ systems which could contain ρ-mesons. And the rich results on electroproduction from Jlab and MAMI are not included. Still, a large variety of reactions is fitted in a coupled channel analysis of pion- or photon-produced reactions.

2 Partial waves parameterization

In the present analysis, high-spin resonances are described by relativistic multi-channel Breit-Wigner amplitudes; important partial waves with low total spin ($J < 5/2$) are described in the framework of a K-matrix/P-vector approach which automatically satisfies the unitarity condition.

The multi-channel amplitude is defined by matrix $\hat{A}(s)$ where the matrix element $A_{ab}(s)$ defines the transition amplitude for state "a" to state "b". For elastic scattering the amplitude is given by

$$\hat{A}(s) = \hat{K}\,(\hat{I} - \mathrm{i}\hat{\rho}\hat{K})^{-1}, \tag{1}$$

where $\hat{K}$ is a K-matrix, $\hat{I}$ is a unitary matrix and $\hat{\rho}$ is a diagonal matrix of the phase spaces. In case of two particle states (for example πN) the phase space is calculated as a simple loop diagram (see Ref. [9]). For '+' states the phase space is equal to:

$$\rho_+(s) = \frac{\alpha_L}{2L+1}\frac{2|\vec{k}|^{2L+1}}{\sqrt{s}}\frac{k_{10}+m_N}{2m_N}\frac{F(k^2)}{B(L,r,k^2)} \tag{2}$$

and for '−' states the phase space is equal to:

$$\rho_-(s) = \frac{\alpha_L}{L}\frac{2|\vec{k}|^{2L+1}}{\sqrt{s}}\frac{k_{10}+m_N}{2m_N}\frac{F(k^2)}{B(L,r,k^2)}, \tag{3}$$

where s is the total energy squared, k the relative momentum between baryon and meson, $\vec{k}$ its three-vector component, k_{10} is the energy of the baryon (with mass m_N) calculated in the c.m.s. of the reaction and the coefficient α_L is equal to:

$$\alpha_L = \prod_{n=1}^{L}\frac{2n-1}{n}. \tag{4}$$

For regularization of the phase volume at large energies we used a standard Blatt-Weisskopf form-factor with $r = 0.8$ fm and a form-factor $F(k^2)$ using two different forms:

$$F(k^2) = \frac{\Lambda+0.5}{\Lambda+k^2}, \qquad F(k^2) = \frac{\Lambda+2.5}{\Lambda+s}. \tag{5}$$

Fits with both parameterizations produced very similar results. The parameter Λ was fixed from our previous analysis[10, 11] and was not varied in the present fit. For the first parameterization it was taken to be equal to 1.5 and for the second one 3.0.

The exact formulas for the three-body phase volume are given in Ref. [9].

The photoproduction amplitude can be written in the P-vector approach. Here the P-vector amplitude for the initial state "a" photoproduction is then given by

$$A_a = \hat{P}_b\,(\hat{I} - \mathrm{i}\hat{\rho}\hat{K})^{-1}_{ba}. \tag{6}$$

The production vector $\hat{P}$ and the K-matrix $\hat{K}$ have the following parameterizations:

$$K_{ab} = \sum_\alpha \frac{g_a^{(\alpha)} g_b^{(\alpha)}}{M_\alpha^2 - s} + f_{ab},\ \ P_b = \sum_\alpha \frac{g_{\gamma N}^{(\alpha)} g_b^{(\alpha)}}{M_\alpha^2 - s} + \tilde{f}_b, \tag{7}$$

where M_α, $g_a^{(\alpha)}$ and $g_{\gamma N}^{(\alpha)}$ are the mass, coupling constant and photo-coupling of the resonance α; f_{ab} describes a direct (non-resonant) transition from the initial state a to the final state b, e.g. from $\pi N \to \Lambda K$. The production process may have a non-resonant contribution described by $\tilde{f}_b$. In general, these non-resonant contributions are functions of s.

For all partial waves except S_{11}, S_{13} and P_{13} it is sufficient to assume f_{ab} and $\tilde{f}_b$ to be constants. The S_{11} wave requires a slightly more complicated structure. For the scattering amplitudes $\pi N \to N\pi$,

$\pi N \to N\eta$, and $\eta N \to N\eta$ we choose

$$f_{ab} = \frac{f_{ab}^{(1)} + f_{ab}^{(2)}\sqrt{s}}{s - s_0^{ab}}. \quad (8)$$

The $f_{ab}^{(i)}$ and s_0^{ab} are constants which are determined in the fits. For the P_{13} and S_{13} waves such dependence was introduced for the $\pi N \to N\pi$ transition only.

The P-vector approach is based on the idea that a channel with a weak coupling can be omitted from the K-matrix. Indeed, adding to the K-matrix the γN channel would not change the properties of the amplitude. Due to its weak coupling, the γN interaction can be taken into account only once; this is done in the form of a P-vector. Loops due to virtual decays of a resonance into $N\gamma$ and back into the resonance can be neglected safely.

At high energies, the angular distributions exhibit clear peaks in the forward direction of the photoproduced mesons. The forward peaks are connected with meson exchanges in the t-channel. These contributions are parameterized as π, $\rho(\omega)$, K or K^* exchanges.

The most straight forward parameterization of particle exchange amplitudes is the exchange of Regge trajectories. The invariant part of the t-channel exchange amplitude can be written as

$$T(s,t) = g_1(t)g_2(t)R(\pm,\nu,t) \quad \nu = \frac{1}{2}(s-u). \quad (9)$$

Here, g_i are vertex functions, and $R(+,\nu,t)$ and $R(-,\nu,t)$ are Reggeon propagators for exchanges with positive and negative signature. Exchanges of π and K have positive, ρ, ω and K^* exchanges have negative signature.

The propagator for pion exchange has the form

$$R_\pi(+,\nu,t) = \frac{e^{-i\frac{\pi}{2}\alpha_\pi(t)}}{\sin\left(\frac{\pi}{2}\alpha_\pi(t)\right)\Gamma\left(\frac{\alpha_\pi(t)}{2}+1\right)}\left(\frac{\nu}{\nu_0}\right)^{\alpha_\pi(t)}, \quad (10)$$

where $\alpha_\pi(t) = -0.014 + 0.72t$ is a function defining the trajectory, ν_0 is a normalization factor (which can be taken to be 1). The Γ-function is introduced in the denominator to eliminate the additional poles at $t < 0$.

The ρ trajectory has a negative signature and the corresponding propagator is equal to

$$R_\rho(-,\nu,t) = \frac{ie^{-i\frac{\pi}{2}\alpha_\rho(t)}}{\cos\left(\frac{\pi}{2}\alpha_\rho(t)\right)\Gamma\left(\frac{\alpha_\rho(t)}{2}+\frac{1}{2}\right)}\left(\frac{\nu}{\nu_0}\right)^{\alpha_\rho(t)}. \quad (11)$$

where $\alpha_\rho(t) = 0.50 + 0.85t$. The ω trajectory is identical to the ρ trajectory.

3 Elastic $\pi N \to \pi N$ scattering

For πN elastic scattering in low partial waves – with πN in the total spin $J = \frac{1}{2}, \frac{3}{2}$ – we rely on the detailed work of the George-Washington Center for Nuclear Studies[8]. An example of the description of these data with one of the latest solutions is given in Table 1.

Table 1. Pion induced reactions fitted in the coupled-channel analysis and χ^2 contributions. References to the data are given in the text.

$\pi N \to \pi N$	wave	N_{data}	w_i	χ^2/N_{data}
	S_{11}	126		1.40
	S_{31}	102		2.37
	P_{11}	110		2.24
	P_{31}	118		3.23
	P_{13}	108		2.57
	P_{33}	130		5.01
	D_{13}	106		5.06
	D_{33}	136		4.01
$\pi^- p \to \eta n$	$d\sigma/d\Omega$	288		2.76

4 Photoproduction of single neutral pions off protons

The single pion production is dominated by the production of $\Delta(1232)$, $D_{13}(1520)$, $F_{15}(1680)$, $S_{11}(1535)$ and t-channel exchanges at high energies. A typical description of the data is shown in Fig. 1. The description of the single neutral pion photoproduction data is given in Table 2.

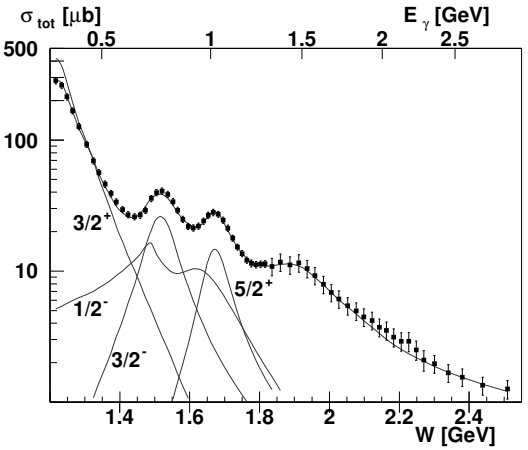

Fig. 1. Contributions of $\Delta(1232)P_{33}$ $D_{13}(1520)$, $S_{11}(1535)$, $S_{11}(1650)$ and $F_{15}(1680)$ to the single neutral pion photoproduction.

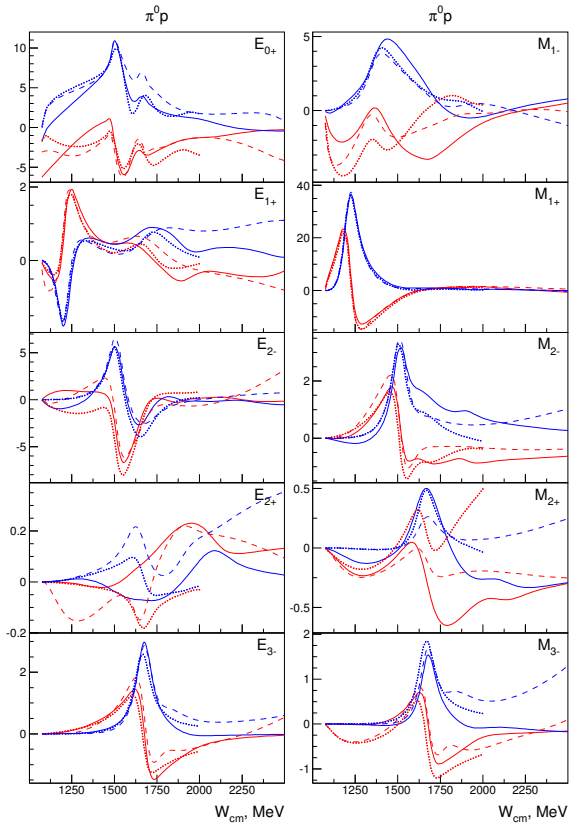

Fig. 2. Multipoles for the $\gamma p \to \pi^0 p$ reaction. Solid curves show our current solution, dashed lines correspond to the SAID solution and dotted lines to the MAID solution. The red curves corresponds to the real part and blue curves to the imaginary part of the amplitudes.

The contributed resonances to this reaction are well known and have 4-star classification by PDG. However different analyses provide different behavior of the amplitudes due to difference in the determination of helicity couplings, pole positions and couplings of resonances to other channels. A comparison of multipoles for the single neutron meson photoproduction form our current solution with those obtained by the SAID[12] and MAID[13] groups is shown in Fig. 2.

The reaction $\gamma p \to \pi^+ n$ has a much stronger non-resonant background than photoproduction of the neutral pion. Indeed the pion exchange amplitude which is forbidden in neutral channel is one of the dominant contributions in the charged pion photoproduction. The multipoles for the charged pion are shown in Fig. 3.

4.1 Photoproduction of η mesons off protons

For photoproduction of η mesons, differential cross sections[14—18] and the related beam asymmetry Σ[19, 20] are the only quantities which have been measured so far. Double polarization observables are presently studied intensively at several laboratories but so far no final results have been reported.

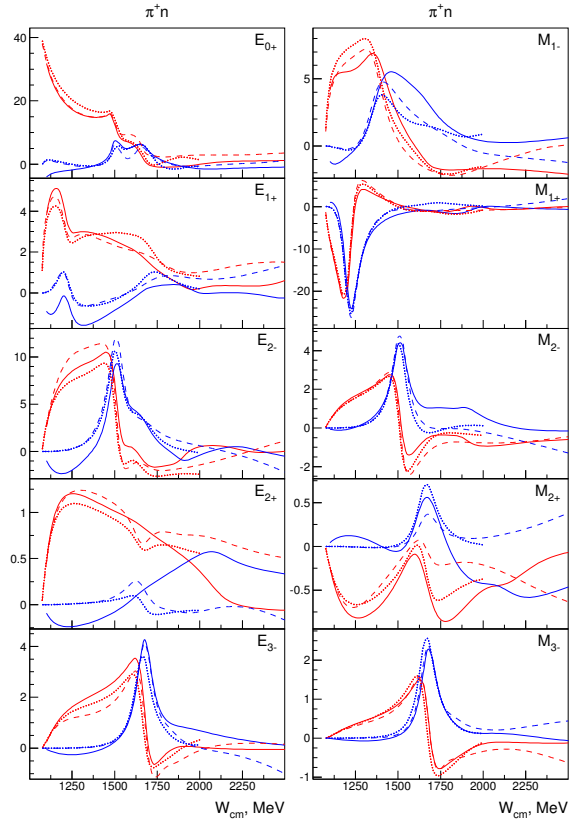

Fig. 3. Multipoles for the $\gamma p \to \pi^+ n$ reaction. Solid curves show our current solution, dashed lines correspond to the SAID solution and dotted lines to the MAID solution. The red curves corresponds to the real part and blue curves to the imaginary part of the amplitudes.

The description of the single eta photoproduction found in our analysis[18] is shown in Fig. 4. Such solution describes unpolarized differential cross section and beam asymmetry data with a very good χ^2. However this solution has problems in the description of the new data which we recently included in the analysis. This is a very clear demonstration about weakness of an analysis with a limited number of fitted reactions.

The solution described rather well the $\pi N \to \eta N$ differential cross section below 1600 MeV measured by Crystal Ball[21] but provided too strong signal in the region 1700 MeV in contradiction with data[22, 23]. As the result we found a new solution with notably suppressed (by the factor 1.5) the ηN coupling for $P_{13}(1720)$. The description of the $\pi N \to \eta N$ data with new (still preliminary) solution is shown in Fig. 5.

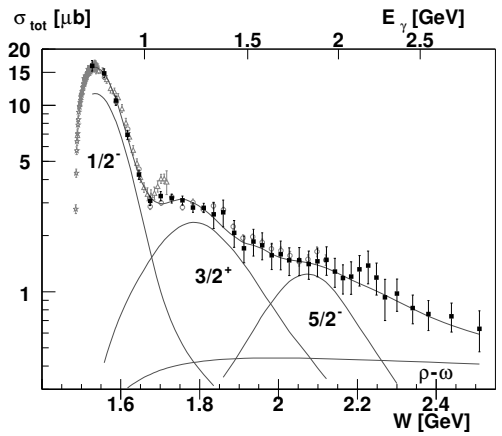

Fig. 4. Contributions of $S_{11}(1535)$ $P_{13}(1720)$, $D_{15}(2070)$ to the single eta photoproduction.

Table 2. Reactions fitted in the coupled-channel analysis and χ^2 contributions. References to the data are given in the text.

	observ.	$N_{\rm data}$	$w_{\rm i}$	$\chi^2/N_{\rm data}$
$\gamma p \to \pi^0 p$	$d\sigma/d\Omega$	1967		1.48
	Σ	1492		3.38
	P	607		3.16
	T	389		4.01
	G	75		2.58
	H	71		1.92
	E	140		1.41
	O_x	7		1.01
	O_z	7		0.38
$\gamma p \to \pi^+ n$	$d\sigma/d\Omega$	1583		1.87
	Σ	899		4.23
	P	252		3.90
	T	661		3.66
	G	75		2.58
	H	71		1.92
	E	231		2.49
$\gamma p \to \eta p$	$d\sigma/d\Omega$	767		1.15
	Σ	151		2.02
	T	50		1.52
$\gamma p \to K^+ \Lambda$	$d\sigma/d\Omega$	1377		1.80
	Σ	111		2.31
	P	202		2.31
	T	66		2.11
	C_x	160		1.22
	C_z	160		1.53
	O_x	66		1.40
	O_z	66		1.86
$\gamma p \to K^+ \Sigma$	$d\sigma/d\Omega$	1289		2.68
	Σ	97		0.86
	P	95		1.56
	C_x	94		2.29
	C_z	94		2.19
$\gamma p \to K^0 \Sigma^+$	$d\sigma/d\Omega$	208		1.51
	P	72		0.72

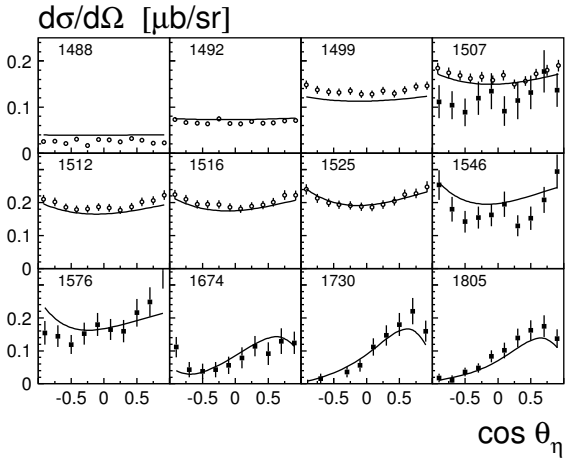

Fig. 5. The description of the $\pi^- p \to \eta n$ data with our current solution.

An additional restriction comes from the fit of target asymmetry data on eta photoproduction. These data have a very peculiar feature at the region of 1500 MeV where target asymmetry shows wavelike angular dependence which can not be explained if $D_{15}(1520)$ state behaves like a usual Breit-Wigner state. Due to this problem these data were considered doubtful in some analyses and excluded from the data base. In our present analysis we also could not describe the wavelike behavior of the target asymmetry in the 1500 MeV region. However we believe that these data provide an important information for the region of 1700 MeV and should be included in the fit. The target asymmetry which behaves rather flat in the region of 1700 MeV also agreed with the impact from the $\pi^- p \to \eta n$ data: the ηN coupling of the $P_{13}(1720)$ state is reduced by the factor 1.5—1.7. The description of the target polarization with new solution is shown in Fig. 6. In the new solution the loss of intensity in the η photoproduction around 1700 MeV is compensated by the S_{11} wave. There is no surprise here: this wave is the strongest one in the region below 1650 MeV and a small refinement of the interference between $S_{11}(1535)$ and $S_{11}(1650)$ can easily compensate the loss due to reduction of the contribution from the $P_{13}(1720)$ state.

We should stress that new solution which describes very satisfactory $\pi^- p \to \eta n$ data and the target asymmetry in the energy region higher 1.55 GeV produces a worse description of the differential cross section and beam asymmetry than the solution with the large $P_{13}(1720)$ signal. The χ^2 changes for these variables are given in Table 3. It proves undoubtedly that including additional data is much more important than a very precise description of a limited data set.

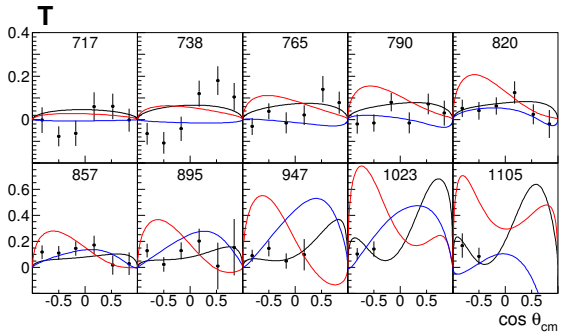

Fig. 6. The description of the target asymmetry with our current solution (black curves). The red curve corresponds to the SAID solution and the blue curves to the MAID solution.

Table 3. The χ^2 for the description of the differential cross section and beam asymmetry with a solution which includes $\pi^-p\to\eta n$ differential cross section and target asymmetry data for the η photoproduction. The numbers in parenthesis correspond to the former solution.

observable	$N_{\rm data}$	$\chi^2/N_{\rm data}$	Exp.
σ(γp→pη)	667	0.92 (0.85)	CB-ELSA
σ(γp→pη)	100	2.72 (1.97)	TAPS
Σ(γp→pη)	51	2.06 (1.81)	GRAAL 98
Σ(γp→pη)	100	2.01(1.43)	GRAAL 04

In all solutions the description of the elastic πN amplitude in the S_{11} channel has a very similar quality. The description of the results obtained by SAID in the energy fixed partial wave analysis is shown in Fig. 7.

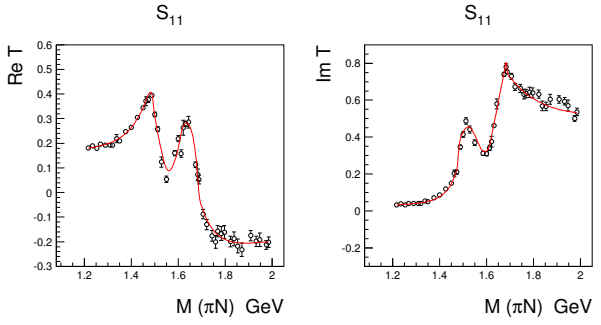

Fig. 7. The description of the elastic S_{11} amplitudes (SAID energy fixed solution) with three pole solution.

Our current solution shows a quite stable pole position for $P_{11}(1710)$. The description of the P_{11} wave is reached with three pole six channel K-matrix. The first pole which corresponds to the Roper resonance is described in details in[24]. The second pole is situated at $M\sim1700$ MeV and $\Gamma\sim160$ MeV and the third pole at $M\sim1870$ and $\Gamma\sim250$ MeV. The description of the P_{11} elastic amplitude (the SAID energy fixed solution) is shown in Fig. 8. The presence of three poles can be easily recognized from the wave like behavior of the real and imaginary parts of the amplitude above 1600 MeV.

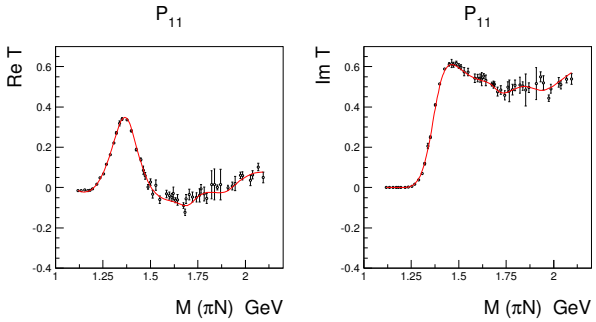

Fig. 8. The description of the elastic P_{11} amplitudes (the SAID energy fixed solution) with three pole solution.

Although the P_{13} wave in the η photoproduction is reduced dramatically in the energy region around 1700 MeV, the new solution shows a clear signal from the $P_{13}(1900)$ which is a good conformation for this state.

5 Channels with open strangeness

A strong signal from the $P_{13}(1900)$ state was observed in the analysis of the double polarization variables C_x and C_z extracted by the CLAS collaboration[25]. The only explanation of this data which was found so far is a contribution from this state. For a combined description of all reactions with open strangeness a contribution from the third pole in the P_{11} partial wave also was necessary. The new solution obtained after including in the data base of the $\pi^-p\to\eta n$ differential cross section and target asymmetry data on η photoproduction hardly changed the description of the channels with open strangeness.

Recent measurements by the GRAAL collaboration made an important step to the complete set of observables for the KΛ and KΣ photoproduction[26]. The description of O_x and O_z observables with the current solution is shown in Figs. 9, 10.

Let us stress that our solution already provided a very good prediction of these data, and a rather good fit was obtained with a very small readjustment of coupling constants only. The quality of the description of the photoproduction reactions with open strangeness can be found in Table 2.

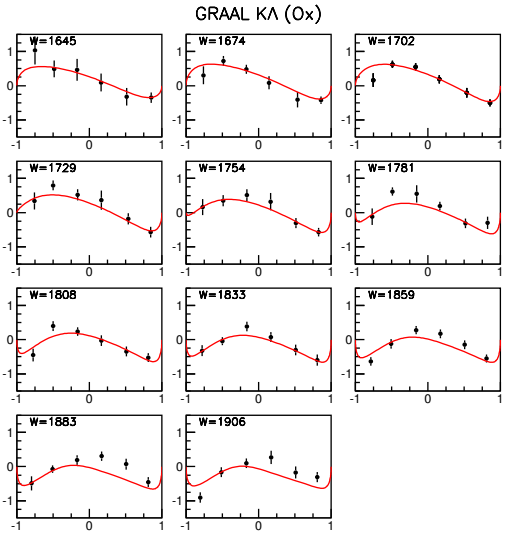

Fig. 9. The description by our current solution of the O_x observable in the $\gamma p \to K\Lambda$ reaction recently measured by the GRAAL collaboration.

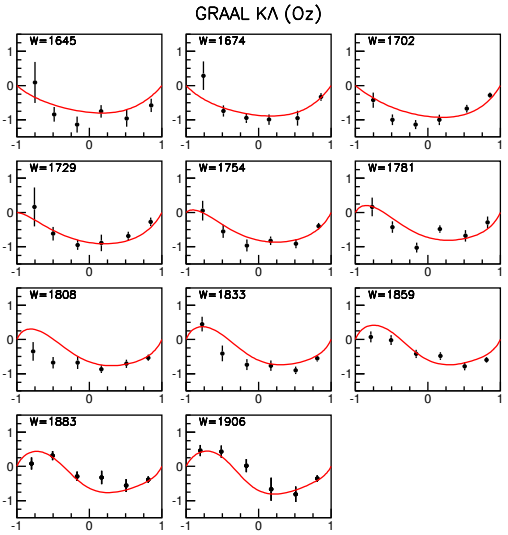

Fig. 10. The description by our current solution of the O_z observable in the $\gamma p \to K\Lambda$ reaction recently measured by the GRAAL collaboration.

6 Multi meson final states

The resonances in the mass region above 1.7 GeV are expected to couple dominantly to the multi meson channels, e.g. $\pi\pi N$ and $\pi\eta N$. A comprehensive study of these final states in the pion induced and photoproduction reactions should reveal new baryon states if they exist. A possibility to perform a combined analysis of single and multi meson final states is the main advantage of our approach. Moreover we analyze reactions with multi meson final states in the framework of the event-by-event based likelihood method which allows us to take accurately into account all correlations between different final channels, e.g. $\Delta(1232)\pi$, $N(1520)\pi$, $N\sigma$.

One of the most interesting reactions is $\gamma p \to \pi^0\eta p$. The dominat final state below 2 GeV is reaction is $\Delta(1232)\eta$ (see Fig. 11 left panel) and therefore provides a good tool to study Δ states in this energy region. Near the $\pi\eta N$ threshold the dominant contribution comes from the $D_{33}(1700)$ state (see Fig. 11 right panel). However this state alone can not describe the contribution of the D_{33} wave into this reaction. At least another D_{33} state in the region 2 GeV is needed to obtain a good description of the data. Another strong partial wave in the region of 2 GeV is the P_{33} partial wave. It has a peak in the region 1900—2000 MeV which corresponds to the well known $P_{33}(1920)$ state. However the pole position for this state is defined with large errors. This is mostly due to presence (or absence) of the $P_{33}(1600)$ state. This resonance is hardly seen in the elastic channel as well as in single photoproduction reactions, and in the $\pi\eta N$ final state it plays the role of low energy background which strongly interferes with $P_{33}(1920)$. It seems that $P_{33}(1600)$ influences rather notably the $\gamma p \to K\Sigma$ reaction: it is quite possible that adding in the analysis the $\pi^+ p \to K\Sigma$ reaction will determine the characteristics of $P_{33}(1600)$ and therefore fix the position of $P_{33}(1920)$. The pole positions for $P_{33}(1920)$ and $D_{33}(1940)$ found in the analysis of the $\gamma p \to \pi^0\eta p$ reaction are given in Table 4.

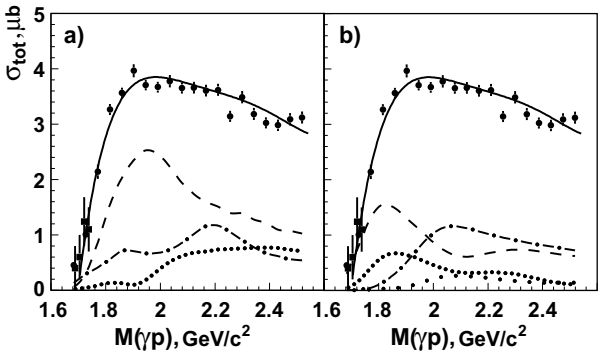

Fig. 11. Left panel: contributions from $\Delta(1232)\eta$ (dashed), $S_{11}(1535)\pi$ (dashed-dotted) and $N\,a_0(980)$ final states. Right panel: D_{33} partial wave (dashed), P_{33} partial wave (dashed-dotted), $D_{33} \to \Delta(1232)\eta$ (dotted) and $D_{33} \to N\,a_0(980)$ (wide dotted).

Table 4. The pole positions and branching ratios for the $\Delta(1920)P_{33}$ and $\Delta(1940)D_{33}$ states.

	$M_{\rm pole}$	$\Gamma_{\rm pole}$
$\Delta(1920)P_{33}$	1980^{+25}_{-45}	350^{+35}_{-55}
$\Delta(1940)D_{33}$	1985 ± 30	390 ± 50

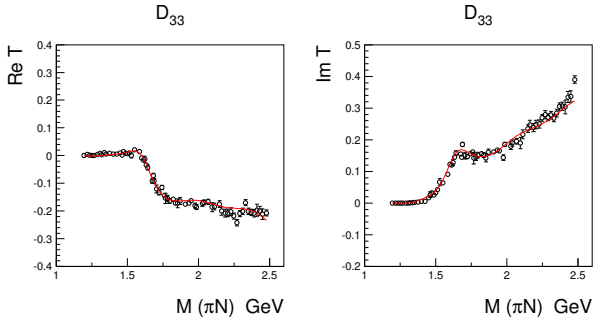

Fig. 12. Description of the SAID energy fixed solution for D_{33} amplitude with 3 pole 5 channel K-matrix.

The description of the SAID energy fixed solution for the D_{33} πN elastic amplitude is shown in Fig. 12. It is seen that the introduction of the $D_{33}(1940)$ state does not contradict the elastic amplitude extracted by SAID.

7 Conclusion

The status of the Bonn-Gatchina partial wave analysis is given in details. The including of the new data on the $\pi^-{\rm p}\to\eta{\rm n}$ and target asymmetry for the η photoproduction reduced by a factor 3-4 the contribution of the $P_{33}(1720)$ state to the η photoproduction reactions. The forthcoming data on the double polarization should resolve ultimately this ambiguity.

The solution with the $P_{13}(1900)$ state which explains the behavior of C_x and C_z asymmetries in the $\gamma{\rm p}\to{\rm K}\Lambda$ and $\gamma{\rm p}\to{\rm K}\Sigma$ reactions is confirmed by the new data measured by GRAAL on the O_x and O_z observables. The analysis of multi particle final states provides an important information about baryon resonances above 1.9 GeV.

References

1 Isgur N, Karl G. Phys. Rev. D, 1979, **19**: 2653; 1981, **23**: 817
2 Capstick S, Isgur N. Phys. Rev. D, 1986, **34**: 2809
3 Glozman L Y et al. Phys. Rev. D, 1988, **58**: 094030
4 Öring U L et al.. Eur. Phys. J. A, 2001, **10**: 395, 447
5 Bijker R, Iachello F, Leviatan A. Annals Phys., 1994, **236**: 69
6 Capstick S, Roberts W. Prog. Part. Nucl. Phys., 2000, **45**: S241
7 Amsler C et al (Particle Data Group). Phys. Lett. B, 2008, **667**: 1
8 Arndt R A, Briscoe W J, Strakovsky I I, Workman R L. Phys. Rev. C, 2006, **74**: 045205
9 Anisovich A V, Sarantsev A V. Eur. Phys. J. A, 2006, **30**: 427
10 Anisovich A V et al. Eur. Phys. J. A, 2005, **25**: 427
11 Sarantsev A V, Nikonov A V, Anisovich A V, Klempt E, Thoma U. Eur. Phys. J. A, 2005, **25**: 441
12 Current solution from http://gwdac.phys.gwu.edu/
13 Drechsel D, Kamalov S S, Tiator L. Eur. Phys. J. A, 2007, **34**: 69 [arXiv:0710.0306]
14 Krusche B et al. Phys. Rev. Lett., 1995, **74**: 3736
15 Dugger M et al (CLAS collaboration). Phys. Rev. Lett., 2002, **89**: 222002; **89**: 249904
16 Crede V et al. Phys. Rev. Lett., 2005, **94**: 012004
17 Bartalini O et al. [arXiv:0707.1385]
18 Bartholomy O et al (CB-ELSA collaboration). Eur. Phys. J. A, 2007, **33**: 133
19 Ajaka J et al. Phys. Rev. Lett., 1988, **81**: 1797
20 Elsner D et al. (CBELSA collaboration and TAPS collaboration). Eur. Phys. J. A, 2007, **33**: 147 [nucl-ex/0702032]
21 Prakhov S et al. Phys. Rev. C, 2005, **72**: 015203
22 Brown R M et al. Nucl. Phys. B, 1979, **153**: 89
23 Richards W B et al. Phys. Rev. D, 1970, **1**: 10
24 Sarantsev A V et al. Phys. Lett. B, 2008, **659**: 94 [arXiv:0707.3591]
25 Schumacher R. Eur. Phys. J. A, 2008, **35**: 299 [arXiv:0802.0985]
26 Lleres A et al (GRAAL collaboration). Eur. Phys. J. A, 2009, **39**: 149 [arXiv:0807.3839]